magnetochemistry

MDPI

Article

Synthesis of a Doped α-Fe_2O_3/g-C_3N_4 Catalyst for High-Efficiency Degradation of Diazinon Contaminant from Liquid Wastes

Tariq J. Al-Musawi [1], Rasoul Asgariyan [2], Murat Yilmaz [3], Nezamaddin Mengelizadeh [4], Abolfazl Asghari [5], Davoud Balarak [6,*] and Mohammad Darvishmotevall [7]

1 Building and Construction Techniques Engineering Department, Al-Mustaqbal University College, Hillah 51001, Babylon, Iraq
2 Department of Environmental, Esfahan Steel Company, Esfahan 8477153111, Iran
3 Department of Chemical Engineering, Faculty of Engineering, Osmaniye Korkut Ata University, 80000 Osmaniye, Turkey
4 Department of Environmental Health Engineering, Evas Faculty of Health, Larestan University of Medical Sciences, Larestan 7433116475, Iran
5 Student Research Committee, Zahedan University of Medical Sciences, Zahedan 9816743463, Iran
6 Department of Environmental Health, Health Promotion Research Center, Zahedan University of Medical Sciences, Zahedan 9816743463, Iran
7 Research Center for Health, Safety and Environment (RCHSE), Alborz University of Medical Sciences, Karaj 3149779453, Iran
* Correspondence: dbalarak2@gmail.com

check for updates

Citation: Al-Musawi, T.J.; Asgariyan, R.; Yilmaz, M.; Mengelizadeh, N.; Asghari, A.; Balarak, D.; Darvishmotevall, M. Synthesis of a Doped α-Fe_2O_3/g-C_3N_4 Catalyst for High-Efficiency Degradation of Diazinon Contaminant from Liquid Wastes. *Magnetochemistry* **2022**, *8*, 137. https://doi.org/10.3390/magnetochemistry8110137

Academic Editor: Huaili Zheng

Received: 28 August 2022
Accepted: 20 October 2022
Published: 22 October 2022

Abstract: In this work, a hematite/porous graphite carbon-nitride (α-Fe_2O_3/g-C_3N_4) catalyst was synthesized through the doping of hematite loaded onto porous graphite carbon-nitride using a heat treatment process. Then, the ability of catalyst was evaluated to degrade diazinon (DZN) for the first time, mainly via the sonophotocatalytic process. Among the samples, the greatest DZN degradation was observed in the sonophotocatalytic system, which separated 100% of DZN from the aqueous solution after 50 min, while the removal percentages for the sonocatalytic, photocatalytic, and adsorption systems were 72.9, 89.1, and 58.1%, respectively. The results of scavengers showed that both sulfate and hydroxyl radicals ($^{\bullet}OH$) participated in removing DZN, although positive holes and negative $^{\bullet}OH$ played a major role. Moreover, the removal efficiencies of the target pollutant using the sonophotocatalytic process were higher than those using the photocatalytic, sonocatalytic, and adsorption processes. The reaction profile followed pseudo-first-order kinetics, and the reaction rate coefficient for the sonophotocatalytic system was 2.2 times higher than that of the photocatalytic system and 2.64 times higher than that of the sonocatalytic system. The energy consumption of the sonophotocatalytic system after 60 min was 11.6 kWh/m^3, while it was 31.1 kWh/m^3 for the photocatalytic system. A DZN removal percentage of 100% was obtained after 50 min under the following conditions: UV intensity of 36 watts, ultrasound frequency of 36 kHz, DZN concentration of 50 mg/L at pH 5, and α-Fe_2O_3/g-C_3N_4 dosage of 0.4 g/L. The catalyst reusability was examined with only a 9.9% reduction in efficiency after eight consecutive cycles. The chemical oxygen demand (COD) and total organic compound (TOC) removal percentages were 95.6% and 88.6%, respectively, and the five-day biochemical oxygen demand (BOD_5)/COD ratio was 0.16 at the beginning of the degradation process and 0.69 at the end of the process. In addition, toxicological experiments showed that degradation of DZN by the sonophotocatalytic process exhibited low toxicity. All results confirmed that the sonophotocatalytic process using α-Fe_2O_3/g-C_3N_4 was a highly efficient process for DZN pollutant removal from liquid wastes.

Keywords: diazinon; sonophotocatalytic; α-Fe_2O_3/g-C_3N_4; characterization analysis; degradation efficiency

1. Introduction

Currently, many pollutants are circulating in the environment, including those that have a toxic nature and can result in a significant impact on human health [1]. The spread of these pollutants is mainly due to the increasing pace of growth in industry, agriculture, and the population. From this point of view, many countries are interested in providing efficient treatments to reduce the concentrations of these pollutants to permissible levels, especially in drinking water and aquatic environments [2]. To achieve this, appropriate treatments must be proposed for the wastewater carrying these pollutants to prevent them from spreading to the environment and becoming difficult to contain. Recently, it was found that the amount of toxins produced to control and prevent plant diseases has increased significantly [3]. Widespread use of phosphorus and chlorine toxins, which cause long-term harmful effects on the ecosystem, is one of the most important factors causing the eutrophication of water, the risk to the life of microorganisms, and damage to the respiratory tract and central nervous system of animals [4,5].

DZN, is one of the routinely used insecticides for insect control in the home environment and agriculture [6]. DZN is a nonsystemic toxin that is stable at an approximate pH of 7; its solubility in water is approximately 40 mg/L at ambient temperature, and it is very easy to digest. The present compound of DZN has low volatility in terrestrial and aqueous media and remains stable for several months in these environments [7,8]. From an environmental perspective, DZN is used in large quantities to improve agricultural yield; thus, it may pollute surface- and groundwater. For all these reasons, DZN is categorized as a class II chemical that poses a relative hazard to humans and aquatic organisms, according to the World Health Organization (WHO) [9].

Therefore, advanced methodologies such as photocatalysis and electrooxidation, as well as traditional methods such as adsorption and biodegradation, have been widely utilized for removing these pollutants [10]. Advanced oxidation processes (AOPs) are effective methods for DZN removal [7,8]. Photocatalytic oxidation (PCO) has been used fruitfully for eliminating pollutants, including DZN [8]. Photocatalytic processes are extremely effective methods that use nanoparticles, leading to full mineralization, absolute decomposition of organic pollutants, and CO_2 production under ambient conditions without producing harmful substances [11,12]. Titanium dioxide (TiO_2) is the most frequently used photocatalyst in photocatalytic studies as it is inexpensive, economical, easy to use, and environmentally friendly [13]. However, the use of TiO_2 photocatalysts in photocatalytic studies has disadvantages, such as difficulty in separation, fast recombination of electrons/holes (e^-/h^+), and a low bandgap [14,15].

As alternative materials, scientists have worked on graphite-based structures such as graphene (G) and graphene oxide (GO), which have large and hexagonal surfaces and can interact strongly with other molecules [16]. Graphite carbon-nitride (g-C_3N_4) is the most stable carbon nitride allotrope, which is employed in the separation and condensation of organic compounds and thus is suitable for these studies. Graphitic carbon-nitride also has features such as low cost, biaxial and porous structure, environmental compatibility, and chemical stability [17]. In addition to these properties of g-C_3N_4, it can undergo rapid recombination due to the active surface electrons; thus, its recycling and isolation are concerns for the environment. To overcome this problem, the g-C_3N_4 photocatalytic activity was upgraded by doping with semiconductor/metallic/nonmetallic elements [18]. To address this, existing g-C_3N_4 has been combined with metal oxide materials such as TiO_2, Tungsten trioxide (WO_3), Zinc oxide (ZnO), and Molybdenum disulfide (MOS_2) by many researchers to form active photocatalysts in the removal of organic pollutants [19,20]. In addition to their nontoxicity, the advantages of applying semiconductor metals in the improvement of treatment agents include high efficiency, ability to work in different environmental conditions, and high chemical stability over a wide pH range [17,18].

Among these semiconductor materials, hematite (α-Fe_2O_3) has attracted great attention; this is related to characteristics such as low cost, optimum bandgap (2.1 eV), low toxicity, and magnetic separation capabilities. α-Fe_2O_3, which is a decent coupling material

for g-C_3N_4, increases the photocatalytic activity under visible light by reducing the photoinduced electron–hole pair recombination rate of the composite after this coupling. According to the literature, there are few studies on the use of α-Fe_2O_3/g-C_3N_4 photocatalysts for degrading dangerous organic pollutants in water [21–23].

Several researchers have suggested that the development of a treatment technology that can create a synergistic effect of activating oxidants will meaningfully increase the removal rate of impurities [24,25]. Sonolysis has come to the fore in recent years, in which ultrasound radiation is adopted because of the absence of chemical involvement as a chemical reaction as well as its safety in use [26,27]. During the sonophotocatalytic process, which is a combination of photocatalysis and sonocatalytic processes, it is possible to generate large numbers of $^{\bullet}OH$ radicals via ultrasound acoustic cavitation [28]. In addition, the catalytic regions are constantly regenerated by the cavitation process, which means the removal of byproducts and the effects of microcurrent and turbulence. In addition, studies have shown that ultrasound radiation can improve the processes of electron transfer, catalyst dispersion, adsorption, and decomposition of the hydrophobic parts of organic compounds when used in a reactor [29]. Few studies have been found in the literature on the toxicity of samples taken from sonophotocatalytic reactors. Dhanasekar et al. used β-$NiMoO_4$ in sonophotocatalytic degradation of methylene blue [30]. Ahmad et al. utilized the sonophotocatalysis process to degrade rhodamine B from aqueous solution [31]. Babu et al. informed the removal of organic compounds by a CuO-TiO_2/rGO/US/UV process [32]. Isari et al. evaluated the sonophotocatalytic degradation of antibiotics by WO_3/CNTs composite [33]. Although most of the cited studies reported adequate efficiency of the present process, little information is available for parameters such as mineralization, toxicity assessment, and energy consumption calculations.

In this article, the recovery of the catalyst and the characteristics of the catalyst are completely carried out, which are rarely discussed in studies; in addition, to the toxicity of the effluent after the process is determined. The amount of energy consumption of fog is one of the most imperative items in recent years, and the amount of biological degradability and the amount of mineralization are also calculated herein. Finally, the kinetics of the reactions are also calculated. Therefore, compared to similar studies, this study is comprehensive, and all aspects are considered.

Therefore, the present study aims to use α-Fe_2O_3/g-C_3N_4 to remove diazinon (DZN). In this study, the operating parameters for DZN removal were optimized. The COD, TOC, and BOD_5 concentrations were also determined for the examination of DZN mineralization levels. Additionally, the reusability of the α-Fe_2O_3/g-C_3N_4 photocatalyst was investigated by performing eight sequential reaction cycles. Finally, a scavenger study was carried out to determine the role of radicals in the degradation.

2. Materials and Methods

2.1. Materials and Reagents

Isopropyl alcohol ($(CH_3)_2CHOH$, >36.0%), ethanol (C_2H_5OH, 99.8%), benzoquinone ($C_6H_4O_2$, >98%), ethylenediaminetetraacetic acid (EDTA, ≥99.7%), melamine (99%), iron(III) nitrate nonahydrate ($Fe(NO_3)_3.9H_2O$, 99.99%), sodium chloride (NaCl, ≥99.5%) and sodium sulfate (Na_2SO_4, ≥99%) were provided by Merck, Germany. DZN (≥95%) was supplied by Sigma Aldrich (St. Louis, MO, USA) and used as the target contaminant. Acetonitrile (CH_3CN, 99.8%) and distilled water for DZN analysis by high-performance liquid chromatography (HPLC) were bought from Merck, Darmstadt, Germany.

2.2. Synthesis of α-Fe_2O_3/g-C_3N_4 Composites

The method employed for synthesizing bulk g-C_3N_4 nanosheets has been described in several previous studies [18]. To synthesize α-Fe_2O_3, a 0.1 M $Fe(NO_3)$ solution was made by dissolving $Fe(NO_3)$ (2.5 g) in 50 mL of DI water. NaOH solution was then instilled into the abovementioned solution, and the solution was stirred for 30 min. NaOH has been found to be a robust precipitating agent compared to KOH. After adding NaOH to

the precursor solution, good mixing with the precursor solution should be considered, which leads to increasing the solution pH and enhancing the reaction rate. The solution pH was adjusted to a value of 8 after adding NaOH. Before the addition of NaOH, the pH of the solution was 7. At this point, the solution was transferred to a Teflon-lined household microwave oven (2.45 GHz) and illumined for 10 min. Then, centrifugation was used to collect the acquired precipitate. The precipitate was washed with DI water and supreme ethanol separately (a few times) and then dried in a vacuum oven at 45 °C. The final product was a light-colored α-Fe_2O_3 nanopowder. During the synthesis of α-Fe_2O_3/g-C_3N_4 nanocomposites, mixing the exact mass proportion (25, 50, and 100 mg) was considered, and the mixture was crushed through the employment of a mortar and pestle for 3 min. It was then placed in a covered alumina crucible and heated using a suppress heater at 400 °C for 4 h. The considered proportions for g-C_3N_4 and α-Fe_2O_3 were 1:0.5, 1:1, and 1:1.5. The names selected for the ultimate products were F, FG1, FG2, and FG3 (indicating products with 0, 25, 50, and 100 mg of g-C_3N_4, respectively).

The catalyst properties were investigated using XRD (XRD, Rigaku D/Max 2500, Tokyo, Japan) with Cu-Ka radiation (k = 0.15418 nm) in a 2θ range of 10–80°, SEM/EDX with a Hitachi S4800 microscope (Tokyo, Japan), UV–Vis diffuse reflectance spectroscopy (HACH, DR5000, Loveland, CO, USA), and FTIR spectroscopy with a Thermo Nicolet Avatar 370 FTIR spectrophotometer (Waltham, MA, USA) by means of the KBr method. Determination of the surface area, total pore volume, and pore distribution of α-Fe_2O_3/g-C_3N_4 was fulfilled via N2 adsorption (−196 °C) by employing a TRISTAR-3000 surface area and porosity analyzer (Micromeritics), and a vibrating sample magnetometer (VSM, Lakeshore 665, Westerville, OH, USA) was utilized.

2.3. Catalytic Experiments

All experiments were executed using UV lamps and ultrasound in a one-liter Pyrex reactor containing a 600 mL sample. In each test, a definite amount of α-Fe_2O_3/g-C_3N_4 was added to the sample containing DZN. The solution pH was adjusted using hydrochloric acid and sodium hydroxide (0.1 N). After each test, 10 mL of the sample was taken using a syringe, and after separation of the catalyst using a magnet, it was injected into the HPLC device. The HPLC device was equipped with a C18 column and UV detector (wavelength of 247 nm). The mobile phase contained 60% acetonitrile and 40% deionized water. The injection rate was 1 mL/min. The amount of mineralization in the sonophotocatalytic system was measured by TOC analysis. Additionally, the amount of biodegradability in the system was obtained using BOD_5, COD, and the ratio between them (COD/BOD_5). The amount of compounds from degradation was also obtained by measuring nitrate, sulfate, ammonium, and phosphate ions.

The degradation efficiency (Efficiency %) of DZN was obtained using Equation (1) [34,35].

$$\text{Efficiency } (\%) = \left[\frac{(C_0 - C_t)}{C_0}\right] \times 100 \quad (1)$$

C_0 and C_t symbolize the DZN initial concentration and the concentration at a specific degradation time (t, minutes), respectively.

The ability of α-Fe_2O_3/g-C_3N_4 to degrade DZN was probed under various conditions. After defining the optimal values of evaluated parameters, sonolysis, sonocatalysis, photolysis, adsorption, photocatalysis, and sonophotocatalysis processes were employed for assessing DZN removal. Recycling experiments for the sonophotocatalyst were conducted using eight consecutive reaction cycles. After each application, catalysts were collected using a magnet. They were then rinsed with ethanol/distilled water (50/50 V/V) to remove impurities. Finally, for reuse, the drying process in an oven was applied at 60 °C for 2 h. Trapping experiments with isopropyl alcohol (IPA), Ethylenediaminetetraacetic acid (EDTA), and p-benzoquinone (BQ) scavengers were performed to categorize the species active in the removal of DZN. Toxicity evaluation of the treated solution was performed by microbial culture of E. coli. In an autoclave, several lactose broth tubes were sterilized.

Incubation of E. coli in Eosin Methylene Blue (EMB) agar medium was done at 37 °C for 24 h. To appraise the toxicity, some tubes were used for the toxicity tests (10 mL of culture medium + 1 mL of reactor output + one microbial loop), and some were used for the control tests (10 mL of culture medium + one microbial loop). After incubation at 37 °C, measuring the absorption of the tubes was fulfilled by a UV–Vis spectrophotometer at 600 nm.

3. Results and Discussion

3.1. Characterization Results

The optical absorption and bandgap of the catalysts were scrutinized through the employment of UV-DRS, and the reflectance diagram is illustrated in Figure 1a. It is clear that all specimens had a stronger absorption in the visible region. The absorption edges for α-Fe_2O_3 and α-Fe_2O_3/g-C_3N_4 were found at 456 and 461 nm, respectively [18]. A shift was observed toward the longer wavelength side. The remarkable redshift detected within the absorption edge is indicative of a reduction in the bandgap of the catalyst. Based on the UV diagram (1b), the bandgap was estimated using the Kubelka-Munk (K-M) relation, and the bandgap was determined to be 2.72, 2.7, 2.53, 2.41, and 2.13 eV for g-C_3N_4, F, FG1, FG2, and FG3, respectively. The smaller bandgap of the FG3 catalyst is due to the combination of the high amount of g-C_3N_4 with α-Fe_2O_3, which induces an imaginable charge transfer between g-C_3N_4 and Fe_2O_3. Since FG3 has a lower bandgap, the study is performed using FG3.

Figure 1c delineates the N_2 adsorption–desorption analysis and the pore size distribution of α-Fe_2O_3 and α-Fe_2O_3/g-C_3N_4 catalysts. It is observed that both samples show type IV isotherms, which indicates the mesoporous nature of the sample [21]. The surface area of α-Fe_2O_3, g-C_3N_4, and α-Fe_2O_3/g-C_3N_4 catalysts are 21.2, 124, and 107 m^2/g, respectively. In addition, the pore size of the α-Fe_2O_3/g-C_3N_4 catalyst is 26 nm. A high surface area of the α-Fe_2O_3/g-C_3N_4 catalyst is desirable to enhance the adsorption reaction.

The morphology and nanostructure of the samples were analyzed by SEM, TEM, and HRTEM, and the SEM results are represented in Figure 1d. As publicized by the SEM, α-Fe_2O_3 was regular and spherical, while the synthesized α-Fe_2O_3/g-C_3N_4 nanocomposite was irregular and had a rugged surface. This could be due to the formation of α-Fe_2O_3 nanoparticles on the g-C_3N_4 catalyst surface [18]. The TEM image of the composite displays the thriving dispersion of α-Fe_2O_3 nanoparticles on the surface of g-C_3N_4 nanosheets, with an average size of 20–30 nm (Figure 1e). The α-Fe_2O_3 particle coating can reduce the aggregation of g-C_3N_4 bulk sheets. The HRTEM image shows that the interfacial distance is approximately 0.36 nm (Figure 1f), which corresponds to the (012) plane of α-Fe_2O_3. The HRTEM image reveals a close relationship between g-C_3N_4 and α-Fe_2O_3, which indicates the formation of the α-Fe_2O_3/g-C_3N_4 composite. Intimate contact between g-C_3N_4 and α-Fe_2O_3 is useful for separating and transporting photogenerated charge carriers [17]. The HRTEM and TEM images confirm the SEM results and show that α-Fe_2O_3 particles are uniformly dispersed on the g-C_3N_4 surface. In addition, the EDX image of the catalyst is publicized in Figure 2a. Based on the mentioned figure, the catalyst is composed of carbon, nitrogen, oxygen, and iron elements.

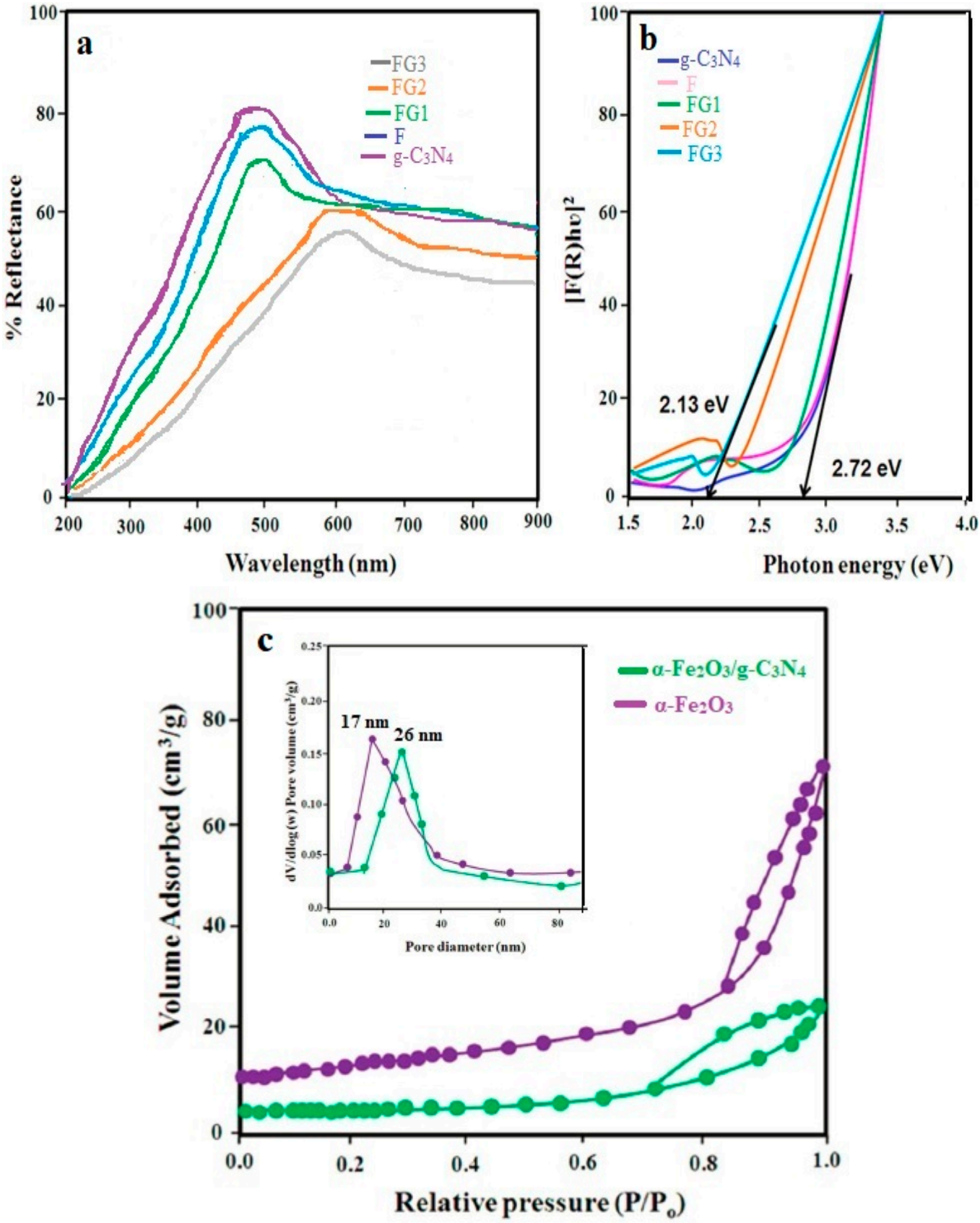

Figure 1. *Cont.*

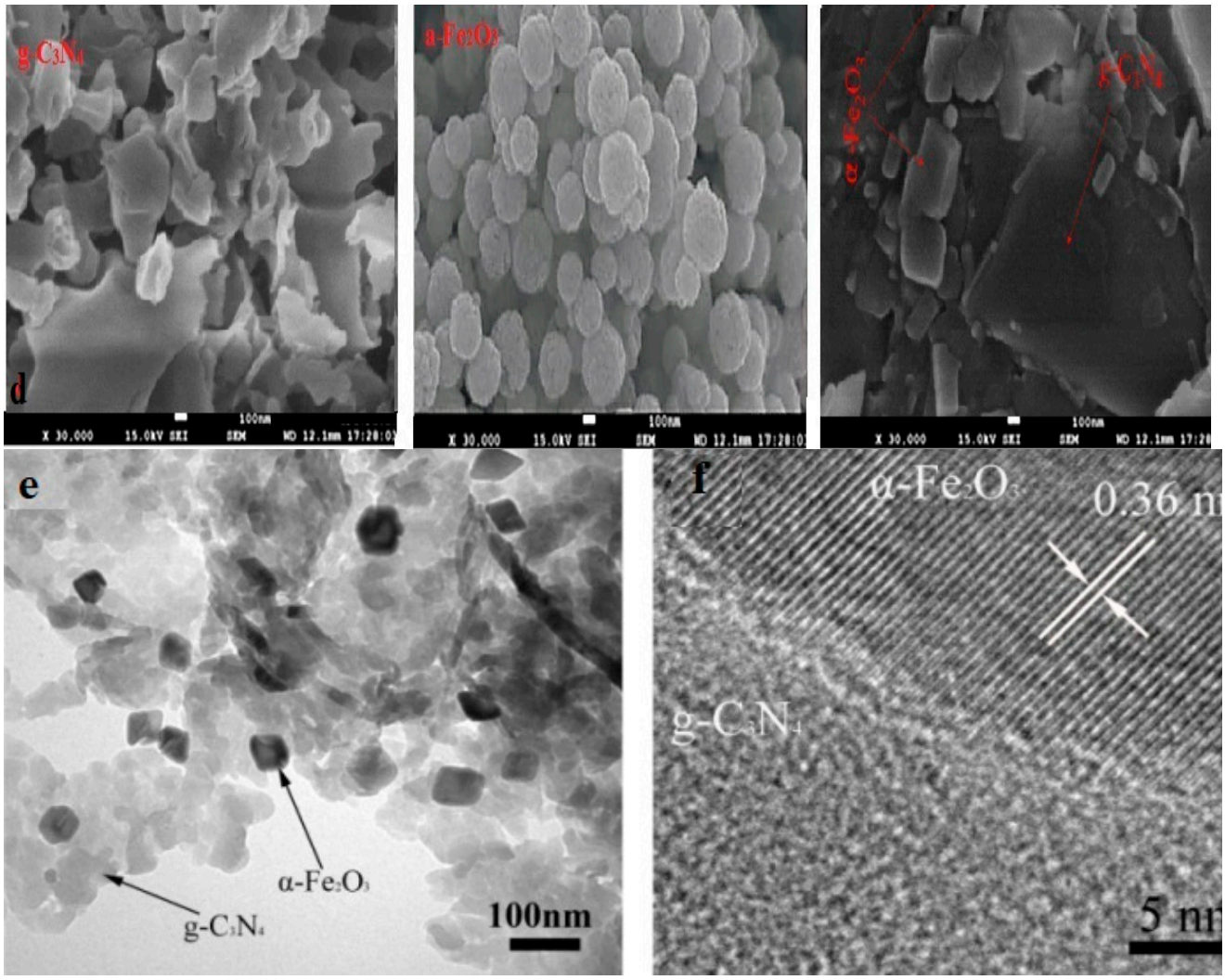

Figure 1. UV–Vis DRS spectra of α-Fe_2O_3/g-C_3N_4 (reflectance spectra) (**a**); plot of transferred Kubelka-Munk versus energy of the light absorbed for g-C_3N_4, F, FG1, FG2, and FG3 (**b**); N_2 sorption isotherms (**c**); SEM images of g-C_3N_4, α-Fe_2O_3, and α-Fe_2O_3/g-C_3N_4 (**d**); TEM image of α-Fe_2O_3/g-C_3N_4 (**e**); HRTEM image of α-Fe_2O_3/g-C_3N_4 (**f**).

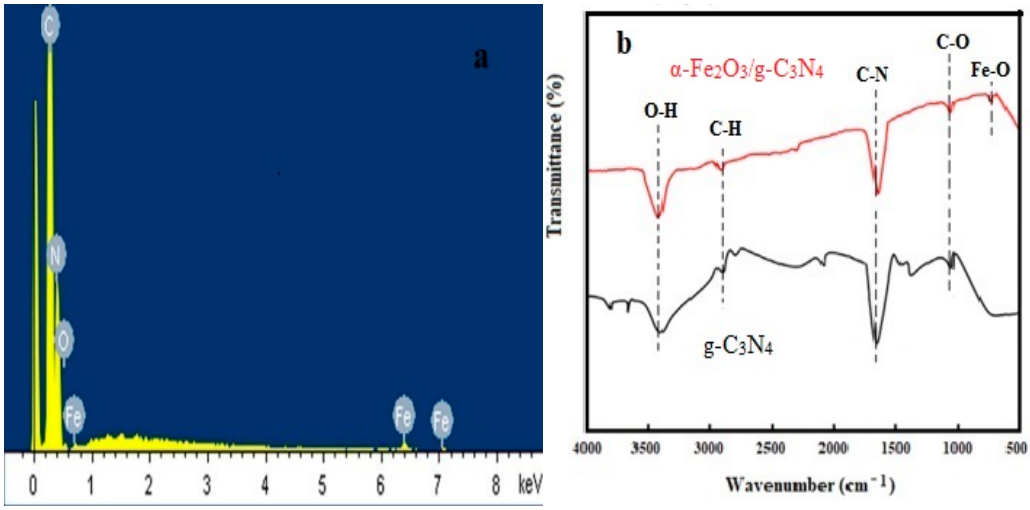

Figure 2. *Cont.*

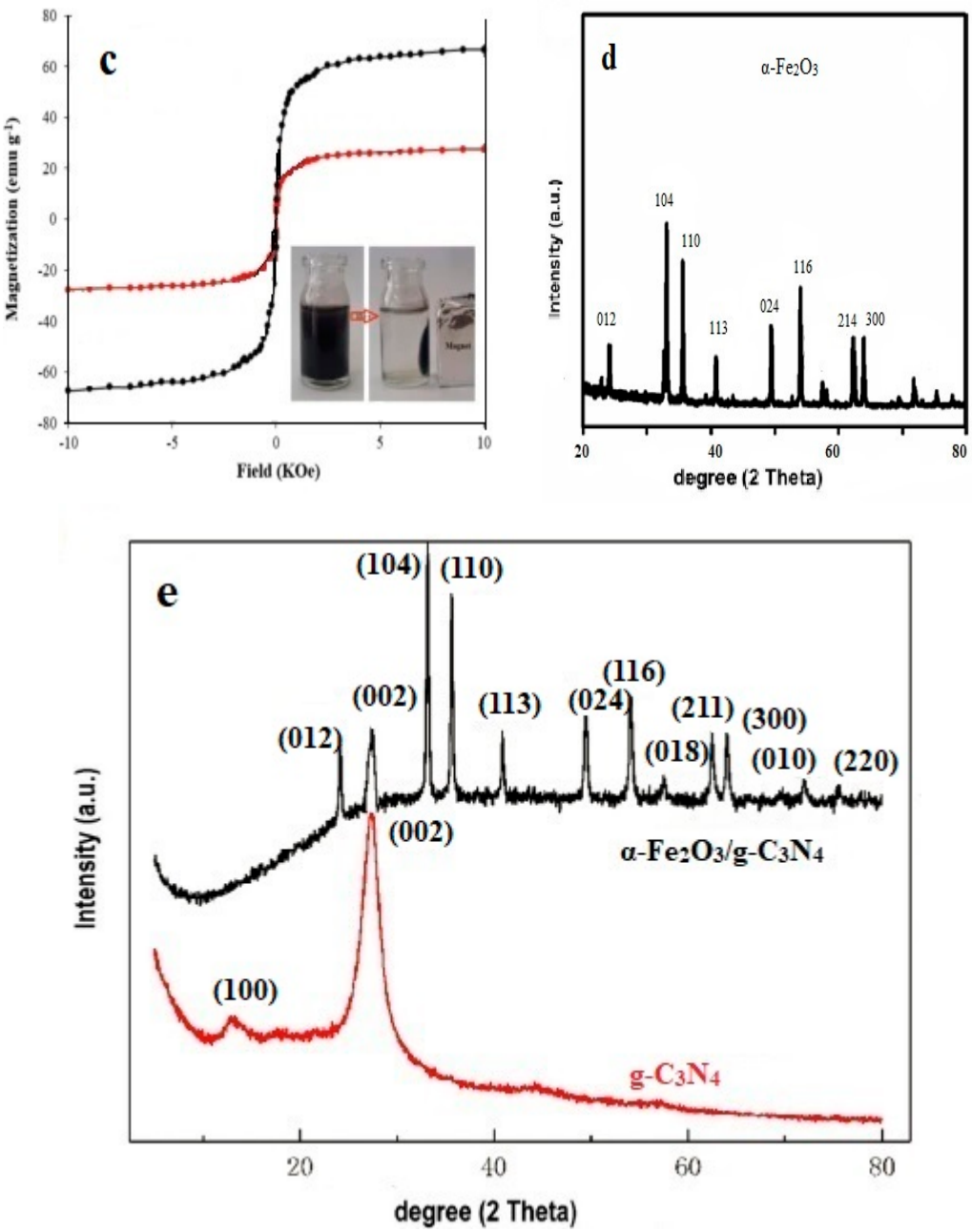

Figure 2. EDX patterns (**a**); IR spectra of g-C_3N_4 and α-Fe_2O_3/g-C_3N_4 (**b**); VSM patterns of α-Fe_2O_3 and α-Fe_2O_3/g-C_3N_4 (**c**); XRD patterns of α-Fe_2O_3 (**d**); and g-C_3N_4 and α-Fe_2O_3/g-C_3N_4 (**e**).

In Figure 2b, FT-IR spectra related to g-C_3N_4 and α-Fe_2O_3/g-C_3N_4 nanocomposites are shown. Similar chemical functional groups were observed, which can be explained by the lack of obvious differences between the two spectra. A wide absorption band is observed at 3446 cm^{-1}; it originates from the O-H stretching vibration of the water molecules adsorbed on the surface of the nanocomposites. An absorption peak was detected at approximately 2900 cm^{-1}, which corresponds to the stretching vibration of C-H [17]. At approximately 1600 cm^{-1}, the characteristic peak of g-C_3N_4 was observed, which is ascribed to the stretching vibration of C-N heterocycles. In Fe_2O_3-doped g-C_3N_4, the mentioned peak was weaker, which is indicative of the alignment of iron ions with C-N aromatic rings. Another peak observed at 1050 cm^{-1} is related to the C-O stretching vibration. At approximately 670 cm^{-1} in the spectrum of the α-Fe_2O_3/g-C_3N_4 nanocomposite, there was a weak peak ascribed to the Fe-O stretching vibration state [21]. The results confirmed the formation

of binary α-Fe_2O_3/g-C_3N_4 nanocomposites due to the successful interaction of iron oxide nanoparticles with pure g-C_3N_4.

Magnetometer vibrating sample (VSM) analysis was performed to evaluate the magnetic properties of the α-Fe_2O_3 and α-Fe_2O_3/g-C_3N_4 catalysts, and the results are presented in Figure 2c. The results of the above analysis showed that the maximum saturation magnet values for α-Fe_2O_3 and α-Fe_2O_3/g-C_3N_4 were 61 and 21.5 g/emu, respectively. Therefore, it can be acknowledged that the catalyst synthesized in the present study has very good magnetic properties for magnetic separation. Based on the reduction in the obtained α-Fe_2O_3 saturation magnetic curve, it is confirmed that α-Fe_2O_3 is located on the surface of the α-Fe_2O_3/g-C_3N_4 catalyst.

The phase structures of α-Fe_2O_3, α-Fe_2O_3/g-C_3N_4, and g-C_3N_4 were assessed by XRD, and the patterns are displayed in Figure 2d,e. The XRD spectrum corresponding to g-C_3N_4 represents two peaks at 27.7° and 13.1°, which belong to the graphitic C_3N_4 hexagonal phase (JCPDS 87-1526). The peak detected at 27.7°, which is related to the g-C_3N_4 (002) plane, is explained by the interlayer stacking of the conjugated aromatic system. The appearance of the peak at 13.1° is related to the g-C_3N_4 (100) plane, which is due to an in-plane structural packing motif. In the XRD spectrum of α-Fe_2O_3, the peaks observed at 24.18°, 33.15°, 35.75°, 40.93°, 49.43°, 54.02°, 57.56°, 62.51°, and 64.05° were related to the (012), (104), (110), (113), (024), (116), (018), (214), and (300) planes of hexagonal α-Fe_2O_3 (JCPDS No. 33-0664), respectively. Peaks of Fe_2O_3 and g-C_3N_4 were also seen in the synthesized nanocomposites, indicating that Fe_2O_3 was doped on g-C_3N_4.

Through XPS, the combination of g-C_3N_4 and α-Fe_2O_3 in the α-Fe_2O_3/g-C_3N_4 composite was inspected. Fe, O, N, and C are elements detected in the XPS spectrum of α-Fe_2O_3/g-C_3N_4 (Figure 3a). The binding energies of C 1s were detected at 284.1, 288.1, and 288.9 eV. They were related to sp2 hybridized C atoms in C-C, C=N, and C=O, respectively (Figure 4b); defect-containing sp^2 hybridized carbon atoms present in the graphitic domains and pure graphitic sites in the CN matrix may be the reason for those binding energies. The binding energies of N 1s were 397.9 eV (assigned to sp2 hybridized N atoms in C=N), 398.9 eV (related to sp^3 hybridized N atoms in C-[N]3), and 400.6 eV (assigned to sp3 hybridized N atoms in C-NHX) (Figure 4c). In Figure 4d, the high-resolution spectrum of O 1s is presented. The binding energies were 531.4 and 527.9 eV, which were related to sp2 hybridized O atoms in C=O and latticed oxygen in α-Fe_2O_3. Moreover, the binding energy of 529.7 eV was observed for lattice oxygen in pure α-Fe_2O_3 (Figure 4e); however, for the binding energy of lattice oxygen in α-Fe_2O_3/g-C_3N_4, a negative shift of 1.8 eV, compared to that of pure α-Fe_2O_3, was detected. As depicted in Figure 4f, the peaks of Fe 2p are at 709.8 and 724.1 eV, which can be found to be Fe $2p_{3/2}$ and Fe $2p_{1/2}$, respectively. According to Figure 4g, the binding energies of Fe2p in pure α-Fe_2O_3 were 710.5 and 725.6 eV [21]. The shift that occurred to low binding energy for Fe 2p is possibly related to the formation of Fe-N. This results in the enhancement of the electron density on the Fe, which is explained by the fact that N has a relatively small electronegativity compared to O; this indicates the possibility of forming chemical bonds between two components instead of a physical mixture [17].

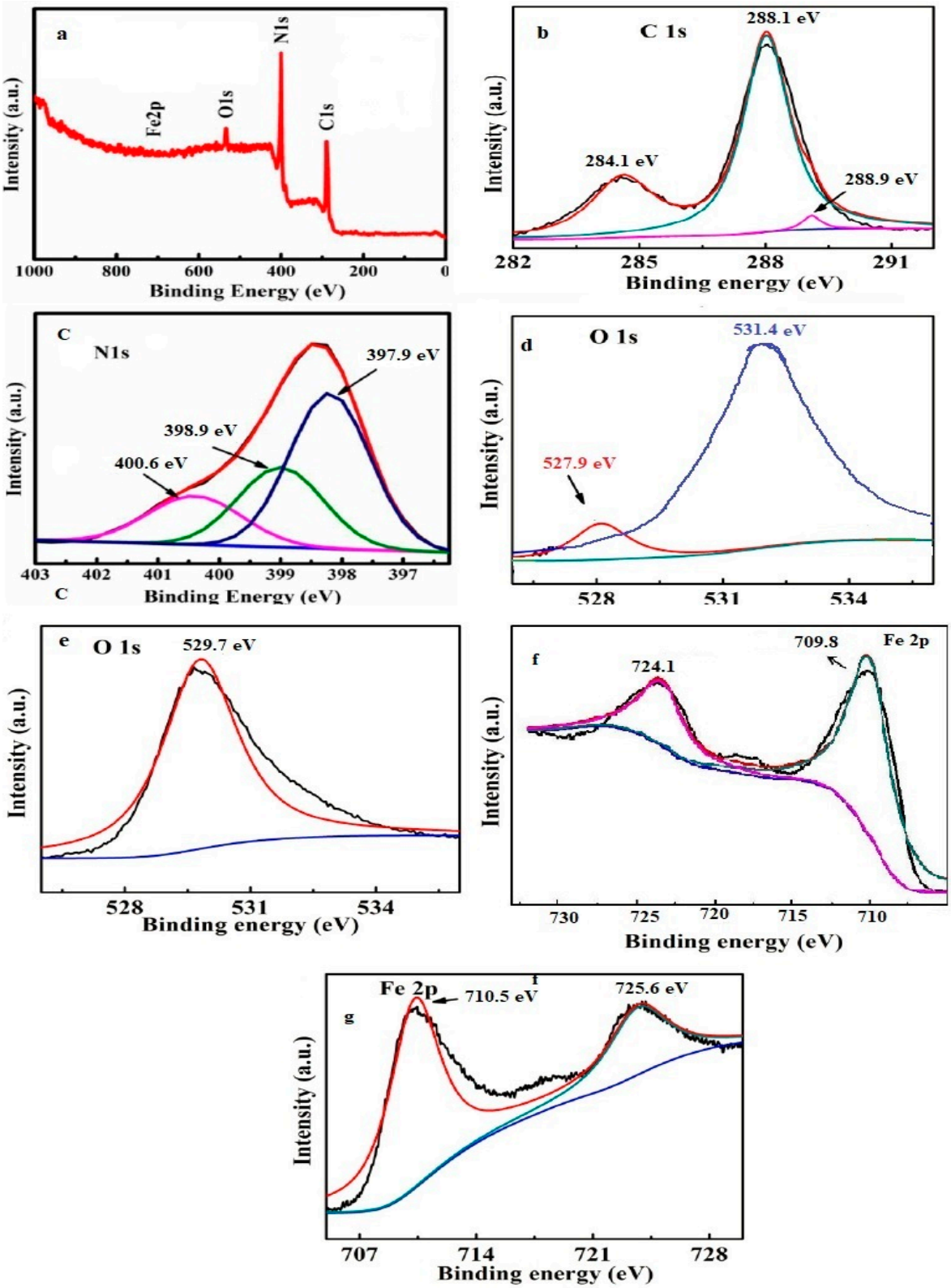

Figure 3. XPS spectra of clean α-Fe_2O_3/g-C_3N_4 (**a**); C 1s (**b**); N 1s (**c**); O 1s (**d**); O 1s α-Fe_2O_3 (**e**); Fe 2p (**f**); and Fe 2p α-Fe_2O_3 (**g**).

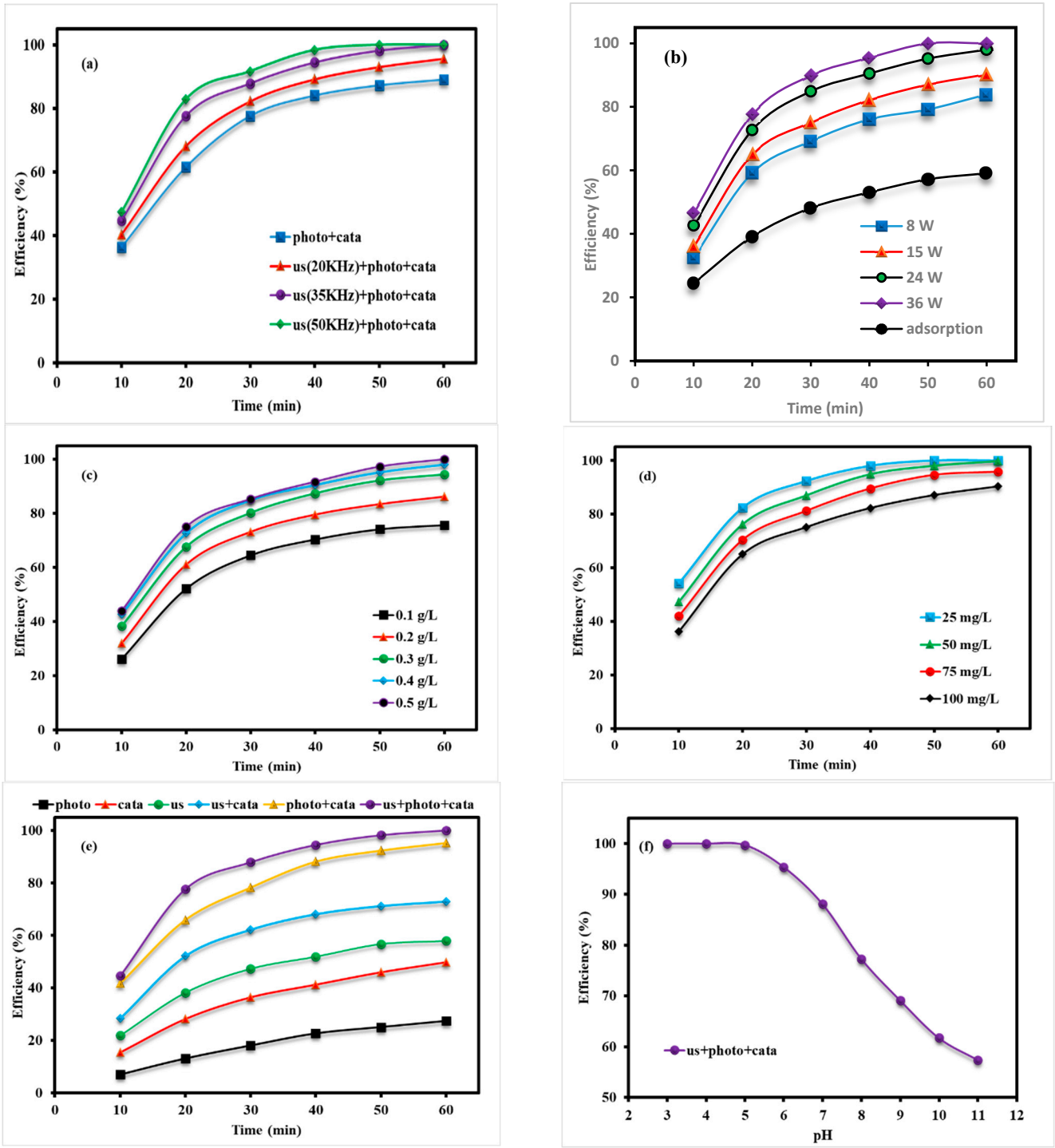

Figure 4. Results of the effect study of different parameters: ultrasonic wave frequency (**a**); UV light intensity (**b**); Fe_2O_3/g-C_3N_4 dose (**c**); initial DZN concentration and contact time (**d**); comparison of the DZN removal efficiencies of the different evaluated treatment systems (**e**); and solution pH (**f**).

3.2. Study of Effects of Operating Parameters

3.2.1. Ultrasonic Wave Frequency

In this study, several experiments were conducted to examine the effect of different ultrasonic wave intensities (20 to 50 kHz) (Figure 4a) (conditions: initial concentration of DZN of 100 mg/L, UV light intensity of 36 W, α-Fe_2O_3/g-C_3N_4 mass of 0.4 g/L, and solution pH of 5). The degradation efficiency of the 100 mg/L DZN solution increased

from 89.7% at 20 kHz to 100% at 50 kHz after 60 min of radiation time. This trend is similar to the work by Liu et al. (i.e., enhancing the percentage of degradation exhibited a direct link to the increase in ultrasonic frequency) [36]. Lim et al. inspected the removal of chlorinated compounds and concluded that the degradation efficiency increased as a result of increasing the frequency from 35 to 300 kHz due to high reactive oxygen species [37]. An increase in the DZN removal by increasing the ultrasonic wave intensity in the obtained results is due to the following reasons: (a) the number of cavitation bubbles is increased [38], (b) the bubbles collapse due to the increase in power, resulting in a large number of $^{\bullet}H$ and $^{\bullet}OH$ radicals produced [39], and (c) the catalyst surface area increases as a result of de-aggregation of α-Fe_2O_3/g-C_3N_4 caused by ultrasonic irradiation [21].

3.2.2. Ultraviolet Light Intensity

Another parameter that is effective in photocatalytic processes is the intensity of ultraviolet light. To examine the effect of ultraviolet light intensity on the system efficiency, experiments were carried out with UV lamps with different powers between 8–36 W (conditions: DZN amount of 100 mg/L, α-Fe_2O_3/g-C_3N_4 mass of 0.4 g/L, solution pH of 5, and ultrasonic waves of 35 kHz). The effect of UV light intensity on DZN degradation under optimum conditions was investigated and is shown in Figure 4b. This figure indicates that when the irradiance is increased from 8 to 36 W within 60 min of irradiation, there is a corresponding clear increase in efficiency from 83.9 to 100%. Electrons are more excited with increasing lamp power. It enhances the number of active $^{\bullet}OH$, which are the main reason for the degradation efficiency of organic pollutants in the photocatalytic treatment systems [40]. The results of the study by Nasirian et al., which investigated the effect of light intensity on the degradation of a dye using the Fe_3O_4/TiO_2/UV catalyst, show a similar trend [41].

3.2.3. Catalyst Dosage

It is stated in most reports that another parameter that has an effect on degradation efficiency in advanced oxidation processes (AOPs) is catalyst dosage [14]. Therefore, in this study, the influence of catalyst dosage changes on the diazinon (DZN) degradation efficiency with a reaction time of 0 to 60 min was evaluated (Figure 4c). This experiment was performed considering constant experimental conditions: UV light intensity of 24 W, DZN amount of 100 mg/L, solution pH of 5, and ultrasonic waves of 35 kHz. The obtained results showed that the degradation efficiency amplified with the increase in the catalyst dose. The detected phenomenon can be explicated by the continuous increase in the formation of active $^{\bullet}OH$ [42]. In addition, Figure 1c indicates that the optimal catalyst dose is 0.4 g/L. The reactor volume and the amount of aqueous solution are effective in determining the optimal dose loading of a catalyst. It is expected that the same optimal α-Fe_2O_3/g-C_3N_4 dosage will be valid for all parameters, since the same reactor is used for all parameters examined in DZN removal. In addition, the DZN degradation efficiency using α-Fe_2O_3/g-C_3N_4 at optimum conditions was compared with the degradation efficiency using only Fe_2O_3 (0.4 g/L). The results showed that α-Fe_2O_3/g-C_3N_4 has a higher ability to degrade DZN molecules than Fe_2O_3 particles, in which the ability of these particles only reached 18.89%.

3.2.4. Initial Diazinon Concentration

The initial concentration of the pollutant is one of the parameters that affect the efficiency of the photocatalytic working system. In this study, the effect of initial diazinon (DZN) concentration was probed under constant operating conditions (α-Fe_2O_3/g-C_3N_4 dose of 0.4 g/L, solution pH of 5, UV light intensity of 15 W, and ultrasonic waves of 35 kHz). Figure 4d shows the effect of a change in the DZN initial concentration on the photocatalytic degradation efficiency. In this study, DZN solutions with concentrations of 25, 50, 75, and 100 mg/L were put into the reactors, and the degradation efficiency of the processes was investigated. According to the results obtained in the presence of a

constant amount of catalyst, since the increase in DZN concentration caused a decrease in the reaction rate, the rate of DZN decomposition decreased. For example, while DZN solution with a 25 mg/L concentration was removed with 100% efficiency after 50 min, DZN solution with an initial concentration of 100 mg/L could be eliminated with 87% efficiency after the same time. The result was possibly due to pollutant adsorption on the catalyst surface [43]. During adsorption, the number of photons present on the catalyst surface decreases. The decrease in the number of photons leads to a decrease in h^+ pairs, which reduces the formation of OH species, which play an active role in the degradation of DZN, thus reducing DZN removal [7].

In the advanced oxidation process (AOP), another parameter that affects the impurity removal efficiency is the reaction time. To examine the effect of time on the efficiency of DZN removal, studies were carried out for 60 min under the optimum conditions obtained in previous experiments. According to the results (Figure 4d), the elimination efficiency is improved with increasing reaction time. The reaction rate was high in the first 20 min of the process, and DZN solution with a 100 mg/L concentration reached a 90.25% removal efficiency at the end of this period. The reason why the reaction rate decreases later on is the short lifetime of $^{\bullet}OH$ radicals, which can only oxidize organic molecules at or near the point of generation [44]. The presence of more impurities at the beginning of the photocatalytic processes will increase the oxidation of $^{\bullet}OH$ radicals, and the yield changes per unit time in the $^{\bullet}OH$ radical formation region will decrease with the decrease in the impurity in the later process. At the end of 50 min, all (100%) of the 25 mg/L DZN solution was removed due to sufficient $SO_4^{\bullet-}$ and $^{\bullet}OH$ production. Due to the technique of oxidation–reduction reactions, it is a commonly established fact that $^{\bullet}OH$ production ends and $SO_4^{\bullet-}$ continues; the free radicals are formed, and pollutants are decomposed [7]. Lin et al. [45] studied the effect of contact time in the ultrasonically activated PS process for phenol removal. According to their results, the percentage of removal increased from 35% to 88% when the mixing time was increased from 10 to 90 min.

3.2.5. Comparative Study of Diazinon Degradation under Different Processes

To survey the effect of different processes on diazinon (DZN) degradation, six different oxidation processes were investigated under optimal conditions from the previous steps, and the results are displayed in Figure 4e. It shows that DZN removal after 60 min was 27.4%, 49.7%, 57.9%, 72.9%, and 95.5% using photons, catalysts, US, US + CATA, and PHOTO + CATA, respectively. However, the removal of 100 mg/L DZN solution resulted in 100% efficiency due to the simultaneous formation of $SO_4^{\bullet-}$ and $^{\bullet}OH$ radicals using the US + PHOTO + CATA hybrid process. As a result, the concurrent use of US, PHOTO, and CATA is very important in terms of energy consumption, as the combination of mentioned methods will reduce the time to attain the highest removal efficiency.

In order to better evaluate the performance of the sonophotocatalytic process based on α-Fe_2O_3/g-C_3N_4, the comparison of the efficiency of the processes in removing different organic pollutants is shown in Table 1. As can be seen, the present study is confirmed by similar studies that α-Fe_2O_3/g-C_3N_4 can be considered as a suitable catalyst for the degradation of pollutants by different oxidation processes. It should be emphasized that the chemical structure of DZN is complex and stable compared to other pollutants in Table 1. Therefore, it is difficult to remove and mineralize it through different processes. In addition, the amount of DZN in our study was 100 mg/L, which was degraded more than 100% in the reaction time of 60 min in the presence of a 0.4 g/L catalyst. Based on the mentioned cases, it can be reported that α-Fe_2O_3/g-C_3N_4 photocatalyst is a promising composite in the degradation of DZN from aqueous solution.

Table 1. The degradation of organic compounds by AOPs based on α-Fe_2O_3/g-C_3N_4.

Pollutant	Catalyst Dose (g/L)	Time (min)	Method	Degradation (%)	Ref.
Bisphenol A (0.5 mM)	0.5	60	Persulfate activation	92.2	[23]
Direct red 81 (0.05 mM)	1.25	120	Photocatalytic	≈80	[46]
Rhodamine B (10 mg/L)	1	120	Photocatalytic	90	[47]
Orange II (50 mg/L)	-	60	Photo-Fenton	≈80	[48]
DZN (100 mg/L)	0.4	60	Sonophotocatalytic	100	Present study

3.2.6. Solution pH

One of the factors affecting the removal of contaminants is the initial pH of the solution. In AOPs, solution pH is extremely effective in the formation of $SO_4^{\bullet-}$ and $^{\bullet}OH$, the stability of oxidants, and the determination of the state and type of iron in the solution [15]. To determine the effect of pH on DZN removal, many experiments were carried out with different values between pH 3 and 11. The results are shown in Figure 4f (conditions: α-Fe_2O_3/g-C_3N_4 dose of 0.4 g/L, initial concentration of DZN of 100 mg/L, ultrasonic waves of 35 kHz, and UV light intensity of 36 W). In the photocatalytic and sonophotocatalytic systems studied for DZN removal, it was concluded that the alkalinity of the aqueous solution decreases the reaction rate, and higher removal occurs under acidic conditions [7]. Charge changes on the catalyst surface naturally affect catalysis, which is a surface phenomenon. In this study, the pH_{PZC} of the catalyst was determined to be 6.7. Consequently, the surface charge of the catalyst is positive when the pH is less than 7 and negative when it is greater than 7. Therefore, the catalyst strongly adsorbs DZN molecules under acidic (pH 3–5) conditions due to the positively charged electrostatic attraction [49]. In the reaction between DZN adsorption molecules and sonophotocatalytic reactive radical species formed on the α-Fe_2O_3/g-C_3N_4 surface, DZN and the catalyst act as a strong Lewis base and a strong Lewis acid, respectively. With decreasing pH, weakened azo bonds are easily broken, and with increasing pH, the rate of degradation decreases due to the negative charges formed between DZN and the catalyst [50].

3.3. Investigation of the Mineralization Behavior of Diazinon

Wastewater treatment has many purposes, the main one of which is to completely decompose pollutants and convert them into biodegradable/safe products. In this work, the analysis of treated DZN-containing solutions in terms of toxicity and mineralization was carried out by a series of test runs. TOC analysis was used to assess the mineralization levels of DZN in the sonophotocatalytic process, and the results obtained are presented in Figure 5a. The graph in Figure 1g shows the degradation and mineralization process of DZN after 120 min under optimal conditions, showing that 100% mineralization did not occur and intermediate products of DZN were formed. The results shown in Figure 1g demonstrate that when the time was increased from 20 min to 120 min, the COD and TOC removal efficiencies were 95.6% and 88.6%, respectively, over time. The fact that the reduction efficiency of TOC is less than the reduction efficiency of DZN is related to the reduction of DZN to less toxic products containing TOC [51]. The TOC and COD concentrations, which were at initial concentrations of 61.9 and 351.2 mg/L, decreased to 7.07 and 15.4 mg/L, respectively, after 120 min. This event indicates that DZN and its intermediates are eventually converted to CO_2 and H_2O in the process studied. As a result, the sonophotocatalysis process is thought to be an operative method for eliminating DZN and its byproducts from aqueous solution, as well as providing appropriate mineralization.

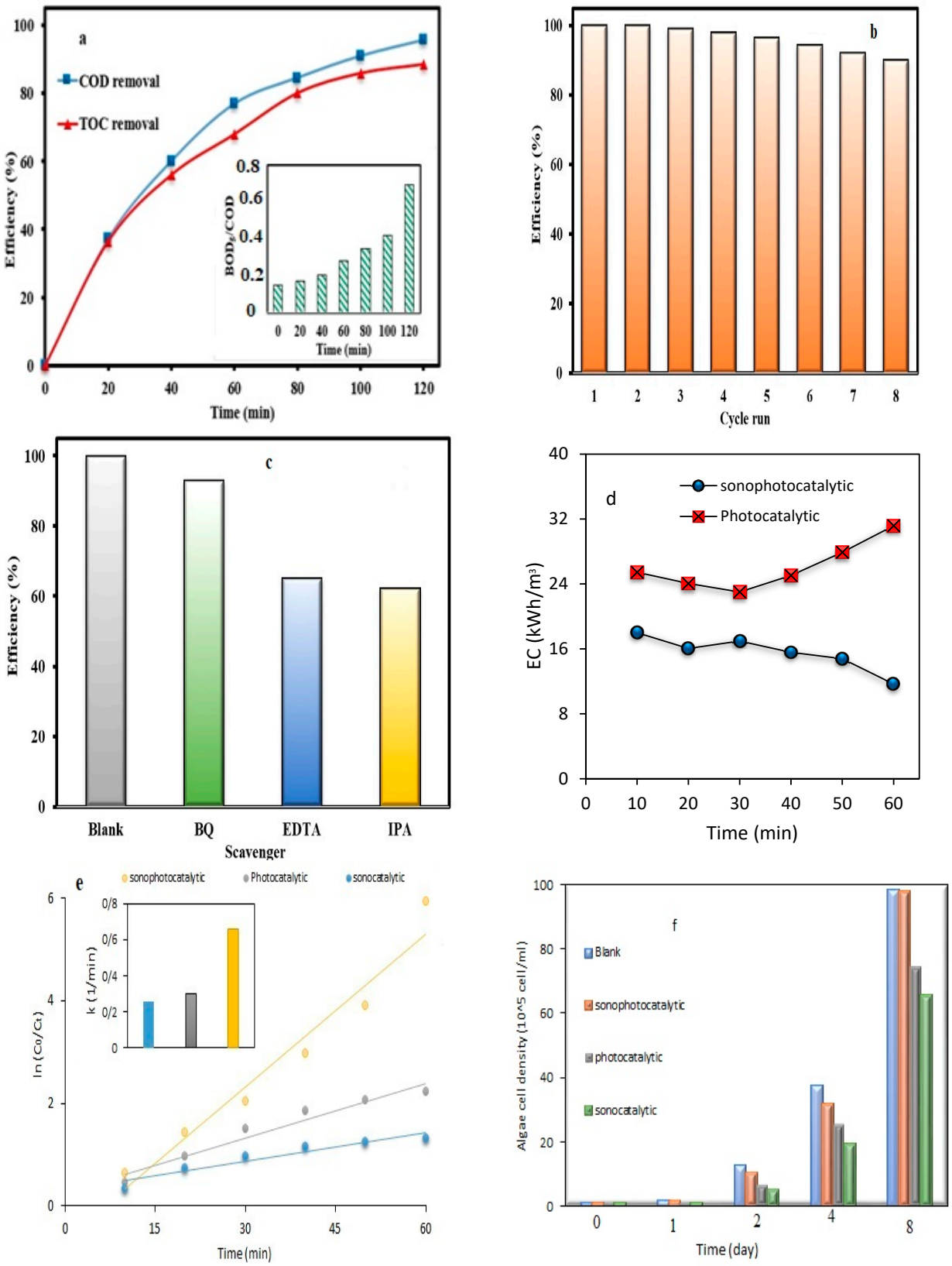

Figure 5. The examination of biodegradability and mineralization (**a**); stability and reusability of the Fe_2O_3/g-C_3N_4 catalyst (**b**); scavenging effect (**c**); energy consumption during sonophotocatalytic and photocatalytic processes (**d**); pseudo-first-order kinetic modelling (**e**); and toxicity test (**f**) of the sonophotocatalytic degradation of DZN.

3.4. Investigation of the Degradation Behavior of Diazinon

The toxicity of wastewater comes first among the parameters that make it difficult to work in biological processes. Industrial waste is not biodegradable, as observed by most scientists. Therefore, industrial wastewater is subjected to advanced treatment processes before being converted into biodegradable wastes [7]. The BOD_5/COD ratio is used to determine this parameter. Wastewater with a BOD_5/COD ratio above 0.4 is considered to be biodegradable [30]. A large number of test runs were carried out under optimum conditions, and the biodegradation behavior of the system was analyzed. Figure 5a shows the experimental results. The biodegradability (BOD_5/COD ratio) of the DZN solution with time showed changes, as shown in Figure 5a. As the reaction time increased from 0 to 120 min, the BOD_5/COD ratio increased from approximately 0.16 to 0.69. Therefore, this improvement in the BOD_5/COD ratio showed that the starting solution is biodegradable as a result of the US + PHOTO + CATA system. Based on the BOD_5/COD results, it can be concluded that the suggested degradation system (sonophotocatalytic process) was efficient in terms of converting the nonbiodegradable DZN molecules into biodegradable byproducts. Therefore, this treatment system can be installed as a pretreatment process before the secondary treatment of industrial or municipal wastewater prior to discharge into the surrounding environment.

In a study by Dbira et al. [52] for tannic acid removal by $UV/S_2O_8^{2-}$ and $US/H_2O_2/Fe^{2+}$, ratios of 0.48 and 0.56 were obtained in effluent $UV/S_2O_8^{2-}$ and $UV/H_2O_2/Fe^{2+}$ systems with a BOD_5/COD initial ratio of 0.2, respectively, and it was concluded that these systems are suitable for the biodegradation of DZN solution.

3.5. The Stability and Reusability of Fe_2O_3/g-C_3N_4

Being stable against metal ion leaching under operating conditions has been known as one of the requirements for employing heterogeneous catalysts in wastewater treatment. Lack of proper stability and continuous and gradual leaching might be associated with the deactivation of the catalyst and further water pollution. In addition to total leaching, the reusability of the catalyst is a critical feature for a heterogeneous catalyst [53,54]. Therefore for checking the reusability, the catalyst was withdrawn from the reaction mixture between each cycle by filtration, washed several times and dried as detailed in the experimental part, and then reused. The results of the studies evaluating the reusability of the synthesized α-Fe_2O_3/g-C_3N_4 are presented in Figure 5b. Experiments were performed under optimal conditions at a concentration of 100 mg/L. As verified by the results obtained, there was a gradual decrease in the catalytic activity of α-Fe_2O_3/g-C_3N_4; therefore, at the end of the eighth cycle, the removal efficiency decreased by only 9.87%. This 9.87% decrease indicates that the synthesized photocatalyst had both good stability and recyclability. Furthermore, after the eighth cycle, it is observed that the iron leaching from the catalysts is less than 10–20 mg, which is a negligible value. The small amount of g-C_3N_4 loss caused the dissociation of the catalytic activator sites, resulting in a loss of catalytic activity [55]. The catalytic activity of the catalyst can be affected by the adsorption of the intermediates, which is due to the fact that its surface can be covered by DZN and the degradation intermediates, resulting in inhibition of the reaction, and the catalyst is used without washing in every study [7].

3.6. Scavenger Test

The most active species generated during the DZN degradation were investigated by scavenging tests in the analysis of the degradation mechanism. Experiments were performed under optimal conditions at a concentration of 100 mg/L. Detection of active species responsible for decolorizing DZN was performed through the employment of capture reagents, e.g., BQ, EDTA, and IPA; the agents mentioned were used for superoxide ($^{\bullet}O_2^{-}$) radicals, holes (h^+), and $^{\bullet}OH$, respectively [16]. $^{\bullet}OH$ radicals were the most effective determinants of color removal of the DZN solution, as seen in Figure 5c. Adding isopropyl alcohol, an $^{\bullet}OH$ scavenger, to the DZN solution resulted in a reduction in the decolorization

rate. However, when other scavengers are added, a decrease in degradation is observed. Therefore, although $^{\bullet}OH$ is the most effective species among the active species, combining these active species might further progress the degradation efficiency [7].

3.7. Determining Energy Consumption

One of the most important factors for evaluating the proficiency of treatment systems is the cost of the system. In recent years, some of the important problems related to treatment methods and comparison of different methods have been energy consumption and costs related to wastewater treatment (per cubic meter of treated wastewater).

The energy consumption (EC) in kilowatt-hours per cubic meter during sonophotocatalytic and photocatalytic processes was estimated through applying the following equation [56,57]:

$$EC = \frac{P \times t}{V \times \log(\frac{C_0}{C_e})} \times \left(\frac{1000}{60}\right) \quad (2)$$

where V refers to the volume of DZN solution in the photochemical reactor, t represents the time taken to treat the solution, and P represents the input power (kW) of the treatment system.

The amount of energy consumed for both systems is shown in Figure 5d. The amount of energy consumed in 60 min for the photocatalytic system to remove 100% of the 50 mg/L DZN solution was 11.6 kWh/m^3, while at the same time and at the same concentration, it was equal to 31.1 kWh/m^3 for the photocatalytic system, and the results show that the energy consumption in the sonophotocatalytic system is lower than that in the photocatalytic system.

In the study piloted by Lin et al. [58] for eliminating phenol by a TiO_2 catalyst, the amount of energy consumption was detected to be 145.5 kWh/m^3, and 80% removal of phenol was observed; the results showed that the amount of energy consumption increases with increasing time. In another study, Kumar et al. utilized ZnO nanoparticles to remove acid black 1 dye, and the energy consumption was equal to 121.2 kWh/m^3 [59]. Yilmaz et al. [10] appraised the removal of acid blue 113 dye and reported that the amount of energy consumption during treatment was calculated between 10 and 60 min; their results were indicative of the fact that with increasing time, the amount of energy consumption increased from 21.2 to 43.4 kWh/m^3. In addition, in the study of Arghavan et al. conducted for the elimination of tamoxifen with $FeNi_3$@SiO_2@ZnO, the amount of energy consumption was calculated at contact between 30 and 120 min; based on their reports, with increasing time, the amount of energy consumption increased from 43.1 to 96.7 kWh/m^3 [60].

3.8. Kinetic Degradation of Diazinon

The chemical reaction kinetics of organic compounds can be expressed by the pseudo-first-order kinetics (PFO) model or the Hinshelwood-Langmuir model. This model is related to the rate of degradation and concentration of organic compounds, which is expressed as Equation (3) [29].

$$r = \frac{dC}{dt} = \frac{K_d k_r C}{1 + KC} \quad (3)$$

where k_r is the original constant rate (1/min) and K_d is the adsorption equilibrium constant (l/mg).

When there is relatively low adsorption or low concentration of organic compounds, Equation (3) can be simplified or expressed as first-order kinetics at a known constant rate (K, 1/min) (Equation (4)).

$$\ln \frac{C_0}{C_t} = -Kt \quad (4)$$

Based on the PFO model, as shown in Figure 5e, the ln C_0/C_e data are drawn against the reaction time as a straight line, while the slope of the diagram shows the rate constant (k). Accordingly, the degradation of DZN by different processes according to the high regression coefficient is performed in accordance with PFO kinetics. In addition, the

reaction rate constant for the sonophotocatalytic system was 0.66, and it was 0.3 and 0.25 1/min for photocatalytic and sonocatalytic systems, respectively; as seen, the rate of DZN degradation by the sonophotocatalytic system is more than double that of other systems. In a study conducted by Al-Musawi et al. for degrading acid blue 113 dye, the results showed that the sonophotocatalytic rate was approximately three to four times higher than that of photocatalytic and sonocatalytic systems [28].

3.9. Toxicological Experiments Using Algal Growth

To evaluate the toxicity of products produced from the degradation of DZN by various sonophotocatalytic, photocatalytic, and sonocatalytic systems, algal growth testing was performed in DZN solution (after one hour of DZN degradation by various processes). Additionally, two solutions were considered, including a solution without DZN and a solution with DZN (50 mg/L). Experiments were performed using the alga Microcystis aeruginosa according to the Organization for Economic Co-operation and Development (OECD) guideline [61]. The test conditions were a light intensity of 8000 lux, a temperature of 20 °C, and an initial alga concentration of 1.1×10^5 cells/mL. The results of algal growth are shown in Figure 5f; except for the sonophotocatalytic process, which exhibited algal growth similar to the DZN-free control solution, there were still toxic compounds in the effluent of other processes (despite reducing the toxicity of the effluent) that inhibited algal growth compared to the control solution. The algae cell density in the control sample increased from 1.1×10^5 to 98.1×10^5 cells/mL, and in the sample of the sonophotocatalytic process, this value was equal to 97.8×10^5 cells/mL, which indicates a significant reduction in toxicity in the effluent. In the untreated DZN sample, the algae cell density decreased after eight days and reached 1.3×10^2. However, in the samples treated with sonocatalytic and photocatalytic processes, the algae cell density reached 65.4×10^5 and 74.3×10^5 cells/mL, respectively, which indicates a significant reduction in toxicity, but the reduction in toxicity was less than that of sonophotocatalytic processes. In a study conducted by Sajjadi et al. for removing DZN by a Fe_3O_4@MOF-2 catalyst, there was a significant reduction in toxicity; however, the toxicity of DZN was not completely eliminated by the photocatalytic process [2].

3.10. Proposed Degradation Mechanism

In order to propose a possible mechanism, the conduction band (E_{CB}) and valence band (E_{VB}) values of α-Fe_2O_3/g-C_3N_4 particles should be determined. The positions of E_{CB} and E_{VB} were determined according to the equations described by Mulliken electronegativity theory (Equations (5) and (6)).

$$E_{CB} = \chi - E_C - 0.5E_g \quad (5)$$

$$E_{VB} = E_{CB} + E_g \quad (6)$$

where E_{CB} and E_{VB} represent the potential of CB and VB particles, χ indicates the electronegativity of the catalyst, E_c demonstrates the energy of free electrons (4.5 eV) in the hydrogen scale, and Eg shows the band gap of the photocatalyst.

According to previous studies [46,62], χ values for Fe_2O_3 and g-C_3N_4 were reported as 5.89 and 4.73 eV, respectively. According to Eg of Fe_2O_3 (2.7 eV) and g-C_3N_4 (2.72 eV) obtained by DRS analysis, the E_{CB} and E_{VB} values were computed, according to the above equations, to be +0.04 and +2.74 eV for Fe_2O_3 and −1.13 and +1.59 for g-C_3N_4, respectively.

Considering our reported results, potential calculations, and earlier studies [7], a possible DZN sonophotocatalytic mechanism is presented in Figure 6. According to this Figure and the suitable surface area of the catalyst, a part of the DZN molecule can be adsorbed on the α-Fe_2O_3/g-C_3N_4 surface. At the same time, under UV light radiation, both Fe_2O_3 and g-C_3N_4 particles can be excited and participate in producing electron-hole pairs. Since VB Fe_2O_3 is more positive than VB g-C_3N_4 and the conduction band of g-C_3N_4 is more negative than Fe_2O_3, the electron in CB g-C_3N_4 is transferred to CB Fe_2O_3, while

the hole is transferred to CB g-C_3N_4 (Equation (7)). This transfer process reduces the electron-hole recombination and advances the charge separation efficiency. In addition, the photogenerated electron on the hematite surface reacts with dissolved oxygen (O_2) to produce $O_2^{\bullet-}$ (Equation (8)) [63]. On the other hand, the holes produced on the g-C_3N_4 surface can react with H_2O and OH^- molecules for producing $^\bullet OH$ (Equation (9)) [28].

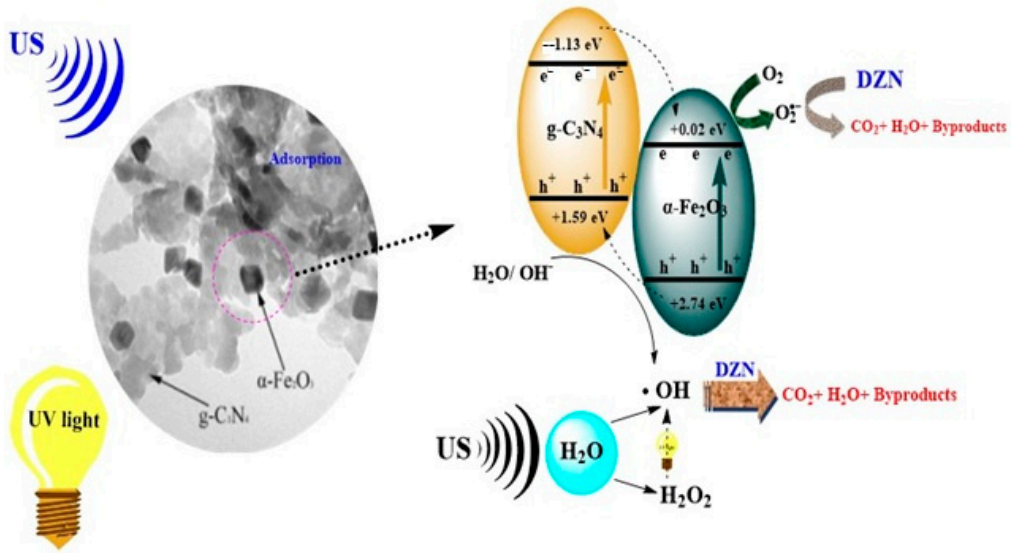

Figure 6. Schematic representation of the mechanism proposed for the α-Fe_2O_3/g-C_3N_4/UV/US system.

In the proposed mechanism, ultrasonic radiation causes the water molecules in the sonophotocatalytic reactor to decompose and release $^\bullet OH$ and H_2O_2 to the environment (Equations (10)–(13)) [64,65]. Meanwhile, the energy required to increase the formation of e−/h+ pairs is provided by catalyst-coupled ultrasonics (Equation (14)). During these steps, UV light degrades H_2O_2 and produces $^\bullet OH$ [66]. Finally, the oxidation of DZN molecules adsorbed on the α-Fe_2O_3/g-C_3N_4 active sites is carried out by the active species (H, $O_2^{\bullet-}$ and h+) (Equation (15)).

$$\alpha - Fe_2O_3/g - C_3N_4 + hv \rightarrow \alpha - Fe_2O_3\left(e^-_{CB}\right) + \ g - C_3N_4\left(h^+\right) \quad (7)$$

$$\alpha - Fe_2O_3\left(e^-\right) + O_2 \rightarrow O_2^{-\cdot} + \alpha - Fe_2O_3 \quad (8)$$

$$g - C_3N_4(h^+) + H_2O/OH^- \rightarrow {}^\bullet OH + g - C_3N_4 \quad (9)$$

$$\text{ultrasound})))) + H_2O \rightarrow {}^\bullet OH + H^\bullet \quad (10)$$

$$H^\bullet + O_2 \rightarrow HO_2^\bullet \quad (11)$$

$$HO_2^\bullet + HO_2^\bullet \ \rightarrow \ H_2O_2 + O_2 \quad (12)$$

$$H_2O_2 + hv \ \rightarrow 2^\bullet OH \quad (13)$$

$$\alpha - Fe_2O_3/g - C_3N_4 + \text{ultrasound})))) \rightarrow \alpha - Fe_2O_3/g - C_3N_4\left(e^- + h^+\right) \quad (14)$$

$$^\bullet OH/h^+/O_2^{\bullet-} + DZN \rightarrow CO_2 + H_2O + \text{degradable byproducts} \quad (15)$$

4. Conclusions

The degradation of diazinon (DZN) was performed using the α-Fe_2O_3/g-C_3N_4 catalyst. The influence of reaction time, initial concentration of DZN, pH, radiation intensity, frequency intensity, and catalyst mass was investigated, and the catalyst characteristics were detected using SEM, BET, XPS, HRTEM, TEM, FTIR, XRD, bandgap, and VSM. The results showed that with increasing reaction time, radiation intensity, and frequency intensity, the percentage of degradation increased, but with increasing pH and DZN amount, the degradation percentage decreased. The removal efficiency of DZN by the sonophoto-

catalytic method (100%) was higher than that of the photocatalytic method (89.1%) and the sonocatalytic method (72.9%). The supermagnetic property of the catalyst enables it to be easily separated from the solution and used in different stages of recovery and reuse so that after eight consecutive reuses, only an approximate 9.9% drop was seen in the degradation of DZN. Experiments on scavengers showed that holes and $^{\bullet}OH$ radicals play a key role in DZN degradation. The results also showed that the simultaneous use of the photo and sono processes significantly reduces energy consumption, and the reaction rate is much higher than that of separate processes. Finally, results showed that the sonophotocatalytic method is more powerful and leads to more efficient and stable results and the formation of less toxic byproducts, compared to photocatalytic and sonocatalytic methods. As our evaluated system could convert nonbiodegradable into biodegradable wastewater, the usefulness of its employment as a pretreatment process before the biological treatment of industrial or municipal wastewater prior to discharge into the ecological system could be anticipated.

Although the present process showed good activity on a batch scale, during the study of the sonophotocatalytic process, some factors remained undiscovered or were kept constant, which requires further study. For example, the adsorption and oxidation mechanisms can be affected by the speed of mixing and the percentage of materials present in the catalyst, so the effect of changes in the speed of mixing and the percentage of catalyst materials needs to be evaluated. Cost analysis is one of the important factors in the success of a new treatment system, as well as its proposal to improve the solution treatment methods. The feasibility of the new system requires a detailed analysis in terms of cost. In this research, the cost details resulting from the results of the laboratory scale will be misleading. Therefore, in the phase of the pilot scale and full scale, a complete study on cost analysis is suggested. In addition, future studies can consider the treatment of emerging persistent pollutants in real solutions to better understand the sonophotocatalytic process.

Author Contributions: D.B. and T.J.A.-M.: conceptualization, investigation data, and collecting, figure analysis, writing—original draft. R.A.: draft writing, correcting, and reading. M.Y.: writing, reading, figure analysis. N.M.: writing—revising and figure analysis. A.A. and M.D.: Data analysis, revising, and editing. All authors have read and agreed to the published version of the manuscript.

Funding: This paper is funded by Zahedan University of Medical Sciences, Zahedan, Iran (code project; 10802).

Institutional Review Board Statement: Not applicable.

Informed Consent Statement: Not applicable.

Data Availability Statement: The data presented in this study are available on request from the corresponding authors.

Acknowledgments: We are grateful to the student research committee of Zahedan University of medical sciences for their financial support (code project; 10802). We would like to appreciate all the fellows of our research group.

Conflicts of Interest: The authors declare no conflict of interest.

References

1. Al-Musawi, T.J.; McKay, G.; Rajiv, P.; Mengelizadeh, N.; Balarak, D. Efficient sonophotocatalytic degradation of acid blue 113 dye using a hybrid nanocomposite of $CoFe_2O_4$ nanoparticles loaded on multi-walled carbon nanotubes. *J. Photochem. Photobiol. A Chem.* **2022**, *424*, 113617. [CrossRef]
2. Sajjadi, S.; Khataee, A.; Bagheri, N.; Kobya, M.; Şenocak, A.; Demirbas, E.; Karaoğlu, A.G. Degradation of diazinon pesticide using catalyzed persulfate with Fe_3O_4@MOF-2 nanocomposite under ultrasound irradiation. *J. Ind. Eng. Chem.* **2019**, *77*, 280–290. [CrossRef]
3. Tariq, N.; Fatima, R.; Zulfiqar, S.; Rahman, A.; Warsi, M.F.; Shakir, I. Synthesis and characterization of $MoO_3/CoFe_2O_4$ nanocomposite for photocatalytic applications. *Ceram. Int.* **2020**, *46*, 21596–21603. [CrossRef]
4. Ayoubi-Feiz, B.; Mashhadizadeh, M.H.; Sheydaei, M. Degradation of diazinon by new hybrid nanocomposites N-TiO_2/Graphene/Au and N-TiO_2/Graphene/Ag using visible light photo-electro catalysis and photo-electro catalytic ozonation: Optimization and comparative study by Taguchi method. *Sep. Purif. Technol.* **2019**, *211*, 704–714. [CrossRef]

5. Al-Musawi, T.J.; Rajiv, P.; Mengelizadeh, N.; Sadat Arghavan, F. Photocatalytic efficiency of $CuNiFe_2O_4$ nanoparticles loaded on multi-walled carbon nanotubes as a novel photocatalyst for ampicillin degradation. *J. Mol. Liq.* **2021**, *337*, 116470. [CrossRef]
6. Zhang, H.; Qiao, J.; Li, G.; Zhang, M.; Li, S.; Wang, J. Construction of coated Z-scheme Pd-$BaZrO_3$@WO_3 composite with enhanced sonocatalytic activity for diazinon degradation in aqueous solution. *Sci. Total Environ.* **2019**, *663*, 97–109. [CrossRef]
7. Al-Musawi, T.J.; Mengelizadeh, N.; Kassim, W.M.S.; Shahbaksh, S. Sonophotocatalytic degradation and operational parameters optimization of diazinon using magnetic cobalt-graphene nanocomposite as a catalyst. *J. Water. Proc. Eng.* **2022**, *46*, 102548. [CrossRef]
8. Tabasideh, S.; Maleki, A.; Shahmoradi, B.; Ghahremani, E.; McKay, G. Sonophotocatalytic degradation of diazinon in aqueous solution using iron-doped TiO_2 nanoparticles. *Sep. Purif. Technol.* **2017**, *189*, 186–192. [CrossRef]
9. Vera, M.; Nyanhongo, G.S.; Guebitz, G.M.; Rivas, B.L. Polymeric microspheres as support to co-immobilized Agaricus bisporus and Trametes versicolor laccases and their application in diazinon degradation. *Arab. J. Chem.* **2020**, *13*, 4218–4227. [CrossRef]
10. Yilmaz, M.; Mengelizadeh, N.; Saloot, M.K.; shahbaksh, S. Facile synthesis of $Fe3O_4$/ZnO/GO photocatalysts for decolorization of acid blue 113 under solar, visible and UV lights. *Mater. Sci. Semicond. Process.* **2022**, *144*, 106593. [CrossRef]
11. Rajiv, P.; Mengelizadeh, N.; McKay, G. Photocatalytic degradation of ciprofloxacin with Fe_2O_3 nanoparticles loaded on graphitic carbon nitride: Mineralisation, degradation mechanism and toxicity assessment. *Int. J. Environ. Anal. Chem.* **2021**. [CrossRef]
12. Balarak, D.; Mostafapour, F.K. Photocatalytic degradation of amoxicillin using UV/Synthesized NiO from pharmaceutical wastewater. *Indones. J. Chem.* **2019**, *19*, 211–218. [CrossRef]
13. Hanh, N.T.; Van Thuan, D.; Khai, N.M.; Thuy, P.T.; Hang, T.T.M.; Vy, N.H.T.; Van Noi, N.; Tran, D.T.; Pham, T.D.; Truc, N.T.T.; et al. Synthesis of Co_3O_4 coated on N,S doped TiO_2 for novel photocatalytic degradation of toxic organic pollutant in aqueous environment. *Ceram. Int.* **2020**, *46*, 21610–21616. [CrossRef]
14. Borji, S.H.; Nasseri, S.; Mahvi, A.H.; Nabizadeh, R.; Javadi, A.H. Investigation of photocatalytic degradation of phenol by Fe (III)-doped TiO_2 and TiO_2 nanoparticles. *J. Environ. Health Sci. Eng.* **2014**, *12*, 101. [CrossRef] [PubMed]
15. Eskandari, N.; Nabiyouni, G.; Masoumi, S.; Ghanbari, D. Preparation of a new magnetic and photo-catalyst $CoFe_2O_4$–$SrTiO_3$ perovskite nanocomposite for photo-degradation of toxic dyes under short time visible irradiation. *Compos. Part B Eng.* **2019**, *176*, 107343. [CrossRef]
16. Balarak, D.; Mengelizadeh, N.; Rajiv, P.; Chandrika, K. Photocatalytic degradation of amoxicillin from aqueous solutions by titanium dioxide nanoparticles loaded on graphene oxide. *Environ. Sci. Pollut. Res.* **2021**, *28*, 49743–49754. [CrossRef] [PubMed]
17. Geng, Y.; Chen, D.; Li, N.; Xu, Q.; Li, H.; He, J. Z-Scheme 2D/2D α-Fe_2O_3/g-C_3N_4 heterojunction for photocatalytic oxidation of nitric oxide. *Appl. Catal. B Environ.* **2021**, *280*, 119409. [CrossRef]
18. Wang, M.; Cui, S.; Yang, X.; Bi, W. Synthesis of g-C_3N_4/Fe_3O_4 nanocomposites and application as a new sorbent for solid phase extraction of polycyclic aromatic hydrocarbons in water samples. *Talanta* **2015**, *132*, 922–928. [CrossRef]
19. John, P.; Johari, K.; Gnanasundaram, N.; Appusamy, A.; Thanabalan, M. Enhanced photocatalytic performance of visible light driven TiO_2/g-C_3N_4 for degradation of diclofenac in aqueous solution. *Environ. Technol. Innov.* **2021**, *22*, 101412. [CrossRef]
20. Zhong, Q.; Lan, H.; Zhang, M.; Zhu, H.; Bu, M. Preparation of heterostructure g-C_3N_4/ZnO nanorods for high photocatalytic activity on different pollutants (MB, RhB, Cr(VI) and eosin). *Ceram. Int.* **2020**, *46*, 12192–12199. [CrossRef]
21. Singh, J.; Basu, S. Synthesis of mesoporous magnetic Fe_2O_3/g-C_3N_4 monoliths for Rhodamine B removal. *Microporous Mesoporous Mater.* **2020**, *303*, 110299. [CrossRef]
22. Zhao, H.; Tian, C.; Mei, J.; Yang, S.; Wong, P.K. Faster electron injection and higher interface reactivity in g-C_3N_4/Fe_2O_3 nanohybrid for efficient photo-Fenton-like activity toward antibiotics degradation. *Environ. Res.* **2021**, *195*, 110842. [CrossRef] [PubMed]
23. Yan, S.; Shi, Y.; Tao, Y.; Zhang, H. Enhanced persulfate-mediated photocatalytic oxidation of bisphenol A using bioelectricity and a g-C_3N_4/Fe_2O_3 heterojunction. *Chem. Eng. J.* **2019**, *359*, 933–943. [CrossRef]
24. Demir, M.; Taymaz, B.H.; Sarıbel, M.; Kamış, H. Photocatalytic Degradation of Organic Dyes with Magnetically Separable PANI/Fe_3O_4 Composite under Both UV and Visible-light Irradiation. *ChemistrySelect* **2022**, *7*, e202103787. [CrossRef]
25. Hu, F.; Sun, S.; Xu, H.; Li, M.; Hao, X.; Shao, G.; Wang, H.; Chen, D.; Lu, H.; Zhang, R. Investigation on g-C_3N_4/rGO/TiO_2 nanocomposite with enhanced photocatalytic degradation performance. *J. Phys. Chem. Solids* **2021**, *156*, 110181. [CrossRef]
26. Arzaee, N.A.; Noh, M.F.M.; Ita, N.S.H.M.; Mohamed, N.A.; Nasir, S.N.F.M.; Mumthas, I.N.N. Nanostructure-assisted charge transfer in alpha-Fe_2O_3/g-C_3N_4 heterojunctions for efficient and highly stable photoelectrochemical water splitting. *Dalton Trans.* **2020**, *49*, 11317–11328. [CrossRef] [PubMed]
27. Vigneshwaran, S.; Jun, B.-M.; Prabhu, S.M.; Elanchezhiyan, S.S.; Ok, Y.S.; Meenakshi, S.; Park, C.M. Enhanced sonophotocatalytic degradation of bisphenol A using bimetal sulfide-intercalated MXenes, 2D/2D nanocomposite. *Sep. Purif. Technol.* **2020**, *250*, 117178. [CrossRef]
28. Al-Musawi, T.J.; Mengelizadeh, N.; Taghavi, M.; Shehu, Z.; Balarak, D. Capability of copper-nickel ferrite nanoparticles loaded onto multi-walled carbon nanotubes to degrade acid blue 113 dye in the sonophotocatalytic treatment process. *Environ. Sci. Pollut. Res.* **2022**, *29*, 51703–51716. [CrossRef]
29. Al-Musawi, T.J.; Rajiv, P.; Mengelizadeh, N.; Mohammed, I.A.; Balarak, D. Development of sonophotocatalytic process for degradation of acid orange 7 dye by using titanium dioxide nanoparticles/graphene oxide nanocomposite as a catalyst. *J. Environ. Manag.* **2021**, *292*, 112777. [CrossRef]

30. Dhanasekar, M.; Ratha, S.; Rout, C.S.; Bhat, S.V. Efficient sono-photocatalytic degradation of methylene blue using nickel molybdate nanosheets under diffused sunlight. *J. Environ. Chem. Eng.* **2017**, *5*, 2997–3004. [CrossRef]
31. Ahmad, M.; Ahmed, E.; Hong, Z.L.; Ahmed, W.; Elhissi, A.; Khalid, N.R. Photocatalytic, sonocatalytic and sonophotocatalytic degradation of Rhodamine B using ZnO/CNTs composites photocatalysts. *Ultrason. Sonochem.* **2014**, *21*, 761–773. [CrossRef] [PubMed]
32. Babu, S.G.; Karthik, P.; John, M.C.; Lakhera, S.K.; Ashokkumar, M.; Khim, J.; Neppolian, B. Synergistic effect of sono-photocatalytic process for the degradation of organic pollutants using CuO-TiO_2/rGO. *Ultrason. Sonochem.* **2019**, *50*, 218–223. [CrossRef] [PubMed]
33. Isari, A.A.; Mehregan, M.; Mehregan, S.; Hayati, F.; Kalantary, R.R.; Kakavandi, B. Sono-photocatalytic degradation of tetracycline and pharmaceutical wastewater using WO_3/CNT heterojunction nanocomposite under US and visible light irradiations: A novel hybrid system. *J. Hazard. Mater.* **2020**, *390*, 122050. [CrossRef] [PubMed]
34. Patil, D.R.; Sarode, K.M.; Nerkar, D.M.; Patil, U.D.; Bachhav, S.G.; Sonawane, U.S.; Paliwal, N. Sonocatalytic Degradation of Methylene Blue by MoS_2-RGO Nanocomposites. *Russ. J. Phys. Chem. A* **2021**, *95*, 2530–2537. [CrossRef]
35. Kakavandi, B.; Bahari, N.; Rezaei Kalantary, R.; Fard, E.D. Enhanced sono-photocatalysis of tetracycline antibiotic using TiO_2 decorated on magnetic activated carbon (MAC@T) coupled with US and UV: A new hybrid system. *Ultrason. Sonochem.* **2019**, *55*, 75–85. [CrossRef]
36. Liu, T.; He, F.W.; Zhang, Y.Q. Synergistic Degradation of Acid Scarlet Dyeing Wastewater by the Ultrasound/Fenton Method. *Appl. Mech. Mater.* **2013**, *448–453*, 34–37. [CrossRef]
37. Lim, M.; Son, Y.; Khim, J. Frequency effects on the sonochemical degradation of chlorinated compounds. *Ultrason. Sonochem.* **2011**, *18*, 460–465. [CrossRef]
38. He, Y.; Grieser, F.; Ashokkumar, M. The mechanism of sonophotocatalytic degradation of methyl orange and its products in aqueous solutions. *Ultrason. Sonochem.* **2011**, *18*, 974–980. [CrossRef] [PubMed]
39. Benomara, A.; Guenfoud, F.; Mokhtari, M.; Boudjemaa, A. Sonolytic, sonocatalytic and sonophotocatalytic degradation of a methyl violet 2B using iron-based catalyst. *React. Kinet. Mech. Catal.* **2021**, *132*, 513–528. [CrossRef]
40. Ghosh, S.; Samanta, M.; Sen, D.; Sarkar, S.; Sarkar, S.; Chattopadhyay, K.K. Photocatalytic and sonocatalytic dye degradation by sulfur vacancy rich ZnS nanopowder. *J. Nanoparticle Res.* **2021**, *23*, 160. [CrossRef]
41. Nasirian, M.; Mehrvar, M. Modification of TiO_2 to enhance photocatalytic degradation of organics in aqueous solutions. *J. Environ. Chem. Eng.* **2016**, *4*, 4072–4082. [CrossRef]
42. Isari, A.A.; Payan, A.; Fattahi, M.; Jorfi, S.; Kakavandi, B. Photocatalytic degradation of rhodamine B and real textile wastewater using Fe-doped TiO_2 anchored on reduced graphene oxide (Fe-TiO_2/rGO): Characterization and feasibility, mechanism and pathway studies. *Appl. Surf. Sci.* **2018**, *462*, 549–564. [CrossRef]
43. Khan, M.A.N.; Siddique, M.; Wahid, F.; Khan, R. Removal of reactive blue 19 dye by sono, photo and sonophotocatalytic oxidation using visible light. *Ultrason. Sonochem.* **2015**, *26*, 370–377. [CrossRef] [PubMed]
44. Khataee, A.; Karimi, A.; Zarei, M.; Joo, S.W. Eu-doped ZnO nanoparticles: Sonochemical synthesis, characterization, and sonocatalytic application. *Ultrason. Sonochem.* **2020**, *67*, 102822. [CrossRef] [PubMed]
45. Lin, Y.-T.; Liang, C.; Chen, J.-H. Feasibility study of ultraviolet activated persulfate oxidation of phenol. *Chemosphere* **2011**, *82*, 1168–1172. [CrossRef]
46. Theerthagiri, J.; Senthil, R.A.; Priya, A.; Madhavan, J.; Michael, R.J.; Ashokkumar, M. Photocatalytic and photoelectrochemical studies of visible-light active α-Fe_2O_3– g-C_3N_4 nanocomposites. *RSC Adv.* **2014**, *4*, 38222–38229. [CrossRef]
47. Zhang, H.; Zhu, C.; Cao, J.; Tang, Q.; Li, M.; Kang, P.; Shi, C.; Ma, M. Ultrasonic-assisted synthesis of 2D α-Fe_2O_3@ g-C_3N_4 composite with excellent visible light photocatalytic activity. *Catalysts* **2018**, *8*, 457. [CrossRef]
48. Wang, Z.; Fan, Y.; Wu, R.; Huo, Y.; Wu, H.; Wang, F.; Xu, X. Novel magnetic gC_3N_4/α-Fe_2O_3/Fe_3O_4 composite for the very effective visible-light-Fenton degradation of Orange II. *RSC Adv.* **2018**, *8*, 5180–5188. [CrossRef]
49. Eshaq, G.; Wang, S.; Sun, H.; Sillanpaa, M. Superior performance of $FeVO_4$@CeO_2 uniform core-shell nanostructures in heterogeneous Fenton-sonophotocatalytic degradation of 4-nitrophenol. *J. Hazard. Mater.* **2020**, *382*, 121059. [CrossRef] [PubMed]
50. Saleh, T.A.; Gondal, M.A.; Drmosh, Q.A.; Yamani, Z.H.; Al-yamani, A. Enhancement in photocatalytic activity for acetaldehyde removal by embedding ZnO nano particles on multiwall carbon nanotubes. *Chem. Eng. J.* **2011**, *166*, 407–412. [CrossRef]
51. Al-Musawi, T.J.; Mengelizadeh, N.; Sathishkumar, K.; Mohebi, S. Preparation of $CuFe_2O_4$/montmorillonite nanocomposite and explaining its performance in the sonophotocatalytic degradation process for ciprofloxacin. *Colloid Interface Sci. Commun.* **2021**, *45*, 100532. [CrossRef]
52. Bāzghale, Ā.A.; Mohammad-khāh, A. Sonocatalytic decolorization of methylene blue from aqueous media by La: ZnO/GO nanocomposites. *Res. Chem. Intermed.* **2019**, *45*, 1985–2005. [CrossRef]
53. Bampos, G.; Frontistis, Z. Sonocatalytic degradation of butylparaben in aqueous phase over Pd/C nanoparticles. *Environ. Sci. Pollut. Res.* **2019**, *26*, 11905–11919. [CrossRef] [PubMed]
54. Nasiri, A.; Malakootian, M.; Heidari, M.R.; Asadzadeh, S.N. $CoFe_2O_4$@Methylcelloluse as a New Magnetic Nano Biocomposite for Sonocatalytic Degradation of Reactive Blue 19. *J. Polym. Environ.* **2021**, *29*, 2660–2675. [CrossRef]
55. Pang, Y.L.; Lim, S.; Lee, R.K.L. Enhancement of sonocatalytic degradation of organic dye by using titanium dioxide (TiO_2)/activated carbon (AC) derived from oil palm empty fruit bunch. *Environ. Sci. Pollut. Res.* **2020**, *27*, 34638–34652. [CrossRef] [PubMed]

56. Dbira, S.; Bensalah, N.; Zagho, M.M.; Ennahaoui, M.; Bedoui, A. Oxidative Degradation of Tannic Acid in Aqueous Solution by UV/$S_2O_8^{2-}$ and UV/H_2O_2/Fe^{2+} Processes: A Comparative Study. *Appl. Sci.* **2019**, *9*, 156. [CrossRef]
57. Sharma, A.; Lee, B.-K. Photocatalytic reduction of carbon dioxide to methanol using nickel-loaded TiO_2 supported on activated carbon fiber. *Catal. Today* **2017**, *298*, 158–167. [CrossRef]
58. Lin, S.-H.; Chiou, C.-H.; Chang, C.-K.; Juang, R.-S. Photocatalytic degradation of phenol on different phases of TiO_2 particles in aqueous suspensions under UV irradiation. *J. Environ. Manag.* **2011**, *92*, 3098–3104. [CrossRef]
59. Kumar, K.; Selvam, B. Influence of operational parameters on photomineralization of Acid Black 1 with ZnO. *Desalination Water Treat.* **2010**, *24*, 132–139.
60. Arghavan, F.S.; Al-Musawi, T.J.; Allahyari, E.; Moslehi, M.H.; Nasseh, N.; Hossein Panahi, A. Complete degradation of tamoxifen using $FeNi_3$@SiO_2@ZnO as a photocatalyst with UV light irradiation: A study on the degradation process and sensitivity analysis using ANN tool. *Mater. Sci. Semicond. Process.* **2021**, *128*, 105725. [CrossRef]
61. OECD. *Test No. 201: Freshwater Alga and Cyanobacteria, Growth Inhibition Test*; OECD Publishing: Paris, French, 2011.
62. Moradi, M.; Kakavandi, B.; Bahadoran, A.; Giannakis, S.; Dehghanifard, E. Intensification of persulfate-mediated elimination of bisphenol A by a spinel cobalt ferrite-anchored g-C_3N_4 S-scheme photocatalyst: Catalytic synergies and mechanistic interpretation. *Sep. Purif. Technol.* **2022**, *285*, 120313. [CrossRef]
63. Sun, S.; Ji, C.; Wu, L.; Chi, S.; Qu, R.; Li, Y.; Lu, Y.; Sun, C.; Xue, Z. Facile one-pot construction of α-Fe_2O_3/g-C_3N_4 heterojunction for arsenic removal by synchronous visible light catalysis oxidation and adsorption. *Mater. Chem. Phy.* **2017**, *194*, 1–8. [CrossRef]
64. Abazari, R.; Sanati, S.; Morsali, A.; Kirillov, A.M. Instantaneous sonophotocatalytic degradation of tetracycline over NU-1000@ ZnIn2S4 core–shell nanorods as a robust and eco-friendly catalyst. *Inorg. Chem.* **2021**, *60*, 9660–9672. [CrossRef] [PubMed]
65. Abdurahman, M.H.; Abdullah, A.Z.; Shoparwe, N.F. A comprehensive review on sonocatalytic, photocatalytic, and sonophotocatalytic processes for the degradation of antibiotics in water: Synergistic mechanism and degradation pathway. *Chem. Eng. J.* **2021**, *413*, 127412. [CrossRef]
66. Liu, G.; Ji, J.; Huang, H.; Xie, R.; Feng, Q.; Shu, Y.; Zhan, Y.; Fang, R.; He, M.; Liu, S.; et al. UV/H_2O_2: An efficient aqueous advanced oxidation process for VOCs removal. *Chem. Eng. J.* **2017**, *324*, 44–50. [CrossRef]